Organic & Biomolecular Chemistry

PAPER

View Article Online
View Journal | View Issue

Cite this: *Org. Biomol. Chem.*, 2018, **16**, 5598

Application of a bodipy–C_{70} dyad in triplet–triplet annihilation upconversion of perylene as a metal-free photosensitizer†

Yaxiong Wei, Min Zheng, Qiaohui Zhou, Xiaoguo Zhou * and Shilin Liu

Received 14th June 2018,
Accepted 12th July 2018

DOI: 10.1039/c8ob01410h

rsc.li/obc

A bodipy–C_{70} dyad was synthesized and applied in triplet–triplet annihilation (TTA) upconversion of perylene as a novel metal-free organic photosensitizer. The photophysical processes were investigated by the methods of steady-state UV-Vis absorption and fluorescence spectroscopy, nanosecond time-resolved transient absorption spectroscopy, cyclic voltammetry, and density functional theory calculations. The bodipy–C_{70} dyad showed an increased molar extinction coefficient up to 82 300 mol^{-1} cm^{-1} at 518 nm compared with the C_{70} monomer. With photo-excitation of the bodipy moiety at 532 nm, the intramolecular singlet–singlet energy transfer between bodipy and C_{70} units was efficient with a quantum yield of nearly 100%, and the lowest triplet state of the dyad was subsequently populated *via* ISC of the C_{70} moiety, with a lifetime of *ca.* 80 μs in toluene. Electrochemical investigation suggested that the intramolecular electron transfer of the excited dyad was thermodynamically prohibited in toluene due to the positive ΔG_{CS} for charge-separation. With the presence of perylene in solution as the triplet energy acceptor and emitter, the TTA upconverted fluorescence was observed with a maximum quantum yield of 10.3%. The overall upconversion capability of 4417 M^{-1} cm^{-1} exceeded that of C_{70} approximately two-fold. Moreover, the bodipy–C_{70} dyad also exhibited an enhanced optical stability under intense irradiation. All data indicated that the dyad was another ideal photosensitizer for TTA upconversion of perylene in the fullerene derivative family.

Introduction

Fluorescence upconversion is extensively applied in the fields of photovoltaics,[1–3] photoelectrochemistry,[4,5] photocatalysis,[6,7] and luminescence bioimaging.[8–10] Some upconversion approaches using two-photon absorption dyes, inorganic crystals and rare-earth materials as photosensitizers have been applied for fluorescence upconversion.[11,12] However, the drawbacks of high excitation power, weak absorption of visible light, and low upconversion quantum yield have restricted their applications. Among the upconversion methods, triplet–triplet annihilation (TTA) has attracted increased attention due to its low power density requirement (down to a few mW cm^{-2}) and the relatively high efficiency, since the solar power density at Earth's surface is only *ca.* 100 mW cm^{-2} at AM 1.5.[13,14] In a typical bimolecular TTA upconversion system, a triplet acceptor can be produced by triplet–triplet energy transfer (TTET) from a triplet photosensitizer to the ground state acceptor, and then the TTA of two triplet acceptors yields an excited singlet, emitting the delayed fluorescence.[15,16]

Over the past few decades, a large number of triplet photosensitizers for TTA upconversion have been developed, with those based on transition metals such as Pt(II),[17] Pd(II),[5,18] Os(II),[19] Ru(II),[20] and Ir(II)[21,22] enjoying particular popularity due to their high efficiency of intersystem crossing (ISC) and long-lived triplet states. However, these transition metal complexes are expensive and usually show overly weak absorption in the visible wavelength range. This has motivated the development of metal-free photosensitizers such as bromo- and iodo-bodipy,[23–25] which also exhibit relatively high ISC efficiencies (83%) due to the heavy-atom effect. Recently, some new synthetic triplet photosensitizers without any heavy atoms have been of great importance and worth looking forward to.[26]

Compared to bromo- or iodo-bodipy,[25,27] and the other heavy-atom-free photosensitizers,[26] fullerene as a common spin converter has an ISC efficiency of unity, and the ISC efficiency is basically not reduced after derivatization. Thus,

Hefei National Laboratory for Physical Sciences at the Microscale, iChEM (Collaborative Innovation Center of Chemistry for Energy Materials), Department of Chemical Physics, University of Science and Technology of China, Hefei, Anhui 230026, China. E-mail: xzhou@ustc.edu.cn

†Electronic supplementary information (ESI) available: ^{1}H NMR and HR-MS spectra; dynamic decay curves of intermediates; TTA-UC spectra; absorption and fluorescence spectra of perylene in toluene; optimized molecular geometries of bodipy–C_{70} at the ground and lowest triplet states. See DOI: 10.1039/c8ob01410h

fullerene has an excellent potential ability to play the role of a triplet photosensitizer. Several C_{60}–organic chromophore dyads and triads were synthesized and applied in photodynamic therapy (PDT) or photocatalysis organic reactions.[28–31] Recently, a few new dyads based on bodipy and C_{60} units have been applied as triplet photosensitizers in the investigation of TTA upconversion,[32,33] with bodipy acting as the light-harvesting antenna and the C_{60} unit playing the role of a spin converter.[34] Using these photosensitizers, the TTA upconversion quantum yields of perylene were reported as 2.9% for carbazole–bodipy–carbazole–C_{60}, 2.9% for bodipy–thiophene–C_{60} and 7.0% for bodipy–bodipy–benzene–C_{60}, respectively. Very recently, three new bodipy–C_{60} derivatives have been synthesized as triplet photosensitizers.[35] By adjusting the π-conjugated system of the light-absorbing antenna, the photosensitizers had different visible absorption wavelengths. In the presence of perylene, the highest upconversion quantum yield was determined to be 7.9%.

Unlike the C_{60} derivatives,[32,33,35,36] other important members of the fullerene family, C_{70} and its derivatives, have hardly been used in TTA upconversion. In fact, C_{70} features an ISC efficiency of almost unity, with the lifetime of its triplet state reported as 40–200 μs depending on the experimental conditions.[37–39] The C_{70} monomer was first used as a photosensitizer in the TTA upconversion of perylene and 9,10-bis(phenylethynyl)anthracene.[40] As a result, green-to-blue and red-to-green fluorescence upconversions with quantum yields of 8% and 0.8% were observed, respectively, although the visible absorption of C_{70} was very weak.[41] To the best of our knowledge, no other investigations on the application of C_{70} derivatives in TTA upconversion have been reported.

Herein, a bodipy–C_{70} dyad has been synthesized and applied in the TTA upconversion of perylene as a novel metal-free organic photosensitizer, in which the bodipy moiety (light-harvesting antenna) and the C_{70} unit (spin converter) are connected by a phenyl ring. The molecular structures of bodipy–C_{70}, C_{70}, bodipy-B, and perylene are shown in Scheme 1. The intermolecular unsaturated bonding stacking interaction can be checked by comparing the new sensitizer, bodipy-B and C_{70} itself. The steady-state absorption and fluorescence emission, transient absorption, and TTA-UC fluorescence emission were measured to reveal step-by-step the dynamic processes of the above systems, including the intramolecular energy transfer, electron transfer and ISC of the dyads. Besides obtaining the quantum yield of TTA-UC, an overall description of the kinetic mechanism is proposed for the TTA-UC system using the bodipy–C_{70} dyad as the triplet photosensitizer.

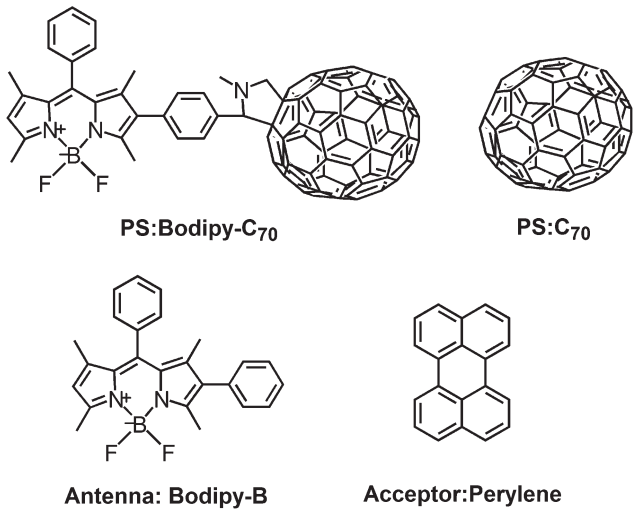

Scheme 1 Molecular structures of triplet photosensitizers (bodipy–C_{70} and C_{70}), the light-harvesting antenna (bodipy-B), and the triplet acceptor (perylene).

Results and discussion

Design and synthesis of the bodipy–C_{70} dyad

As another important member of the fullerene family, C_{70} has a very similar ISC efficiency of almost unity to C_{60}. Thus, the bodipy–C_{70} dyad is expected to exhibit good performance in TTA upconversion as a new triplet photosensitizer, where bodipy acts as the light-harvesting antenna and the C_{70} unit plays the role of a spin converter. Similar to the well-known kinetic mechanism of the bodipy–C_{60} dyad,[35] the singlet–singlet energy transfer between the photoexcited bodipy moiety and the C_{70} unit (as an energy acceptor) probably occurs after light irradiation, followed by ISC of the C_{70} unit to produce the triplet dyad, bodipy–$^3C_{70}$*. In the presence of perylene, the triplet perylene can be formed through TTET in the collision of bodipy–$^3C_{70}$* and perylene. Finally, TTA processes between two triplet perylene molecules produce a singlet and emit the upconverted fluorescence.

All of the compounds were synthesized as shown in the routes in Scheme 2. The ^{1}H NMR and high-resolution mass spectra were used to verify the structure of the synthesized bodipy–C_{70}, and are summarized in the ESI (Fig. S1 and S2†).

UV-Vis absorption and fluorescence emission spectra

Fig. 1(a) shows the steady-state UV-Vis absorption spectra of bodipy–C_{70}, C_{70}, and bodipy-B. The C_{70} monomer exhibited a relatively weak absorption in the visible range, with its maximal molar extinction coefficient ε equaling 20 700 mol^{-1} cm^{-1} at 471 nm. In contrast, bodipy-B featured a strong absorption at 517 nm (ε = 73 100 mol^{-1} cm^{-1}), and the bodipy–C_{70} dyad strongly absorbed at 518 nm (ε = 82 300 mol^{-1} cm^{-1}). Notably, the spectrum of the dyad was slightly different from the sum of the C_{70} and bodipy absorption spectra, indicating that the electronic interactions of bodipy and C_{70} units in the ground state were weak but non-negligible.[28] The sharp peaks at about 460, 380 and 340 nm in the spectra of the C_{70} monomer became blurry and wider for the bodipy–C_{70} dyad. Our theoretical calculations suggested that the derivatization destroyed the conjugated structure of C_{70} a bit, and caused some changes in electronic transitions of the C_{70} moiety. As listed in Table S2 and Fig. S13,† the intense

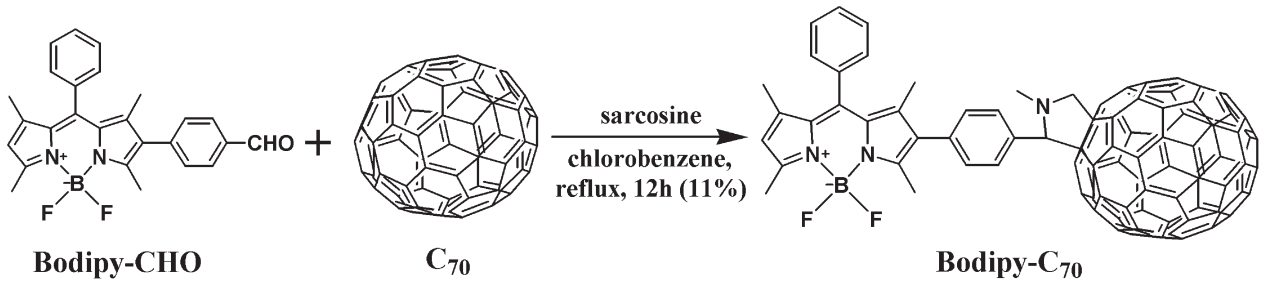

Scheme 2 Synthetic route of bodipy–C_{70} from bodipy-CHO and C_{70}.

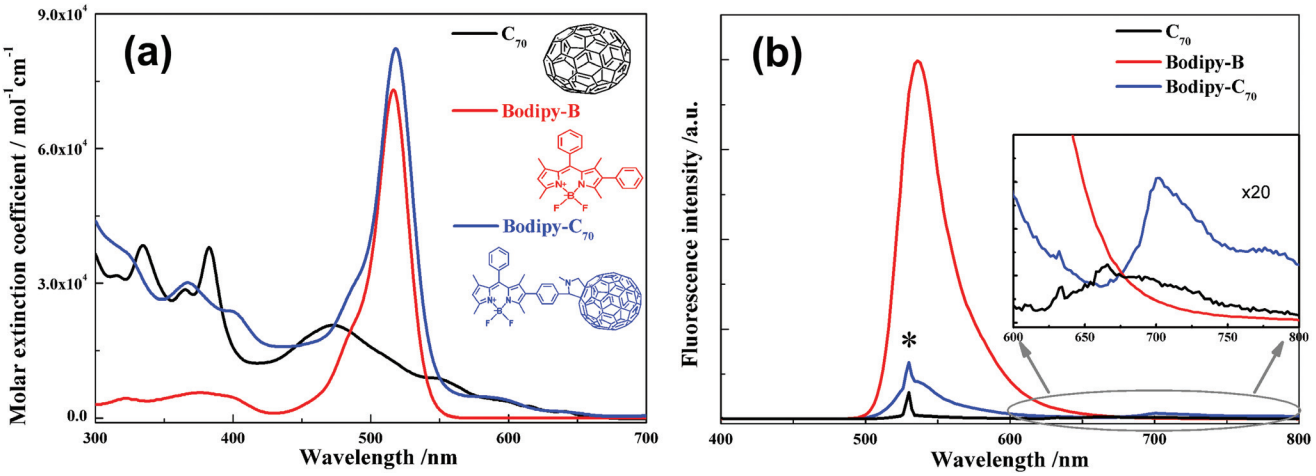

Fig. 1 (a) UV/Vis absorption spectra and (b) fluorescence emission spectra at 532 nm excitation, where the bodipy–C_{70} and C_{70} emission intensities were amplified 20 times. The concentration of the sample was 1.0×10^{-5} M in toluene at 25 °C.

transitions of the C_{70} monomer in the visible range degenerated in the derivatized C_{70} unit of the dyad. As a result, the absorption bands of the C_{70} monomer were visibly broadened and blurred as shown in the experimental spectra.

The fluorescence emission spectra are shown in Fig. 1(b), demonstrating that the antenna, bodipy, featured a strong fluorescence at 536 nm, with those of the bodipy–C_{70} dyad and the C_{70} monomer being very weak. This evidence suggested the occurrence of an efficient energy transfer from the bodipy moiety to the C_{70} unit, similar to the case of bodipy–C_{60}.[33,35] Using the quenched fluorescence intensity, the singlet–singlet energy transfer efficiency from ^{1}bodipy*–C_{70} to bodipy–$^1C_{70}$* was determined to be ~99%. In the magnified spectra of Fig. 1(b), a weak fluorescence emission of C_{70} was observed at 666 nm, and that of bodipy–C_{70} was red-shifted to 702 nm, both of which were the singlet-state emission of the C_{70} unit.[38] The red-shift might be caused by the reduced excitation energy of the C_{70} unit after derivatization. Our calculations also verified the red-shifted absorption of the C_{70} moiety, as shown in Table S2.†

Nanosecond time-resolved transient absorption spectra of the dyad

Fig. 2 shows the nanosecond time-resolved transient absorption spectra of the C_{70} monomer and the dyad, respectively (excitation at 532 nm). The presence of three characteristic absorptions of triplet C_{70} at 415, 593, and 709 nm agreed well with the previous experiments.[34,37–39] A strong ground-state bleaching (GSB) band was observed at 481 nm too, and the intensity of the shoulder at ~438 nm was markedly reduced due to the overlapping of the GSB band. Besides these, a weak peak at 543 nm was observed especially at the beginning of decay as shown in Fig. 2(a). Both dynamic decay behaviors at 438 and 543 nm were very similar to those of the peaks at 415, 593, and 709 nm, indicating that these bands were also contributory to the absorption of triplet C_{70}, *i.e.* these two bands were new characteristic absorptions of triplet C_{70}, being reported here for the first time. As shown in Fig. 2(b), the five positive absorption peaks at 396, 426, 520, 571, and 671 nm were observed for the bodipy–C_{70} dyad. The time-dependent DFT calculations were performed to calculate the absorption spectra of triplet C_{70} and the dyad. As shown in Table S3 and Fig. S14 and S15,† the derivatization of C_{70} broke its perfect symmetry and resulted in changes in triplet–triplet transitions of the C_{70} moiety. The major absorptions of the C_{70} monomer in the visible region were blue-shifted more or less after derivatization. Thus, the peaks of the dyad could be ascribed to the triplet–triplet absorptions of the $^3C_{70}$* unit in the dyad. In other words, the triplet dyad is naturally formed through the

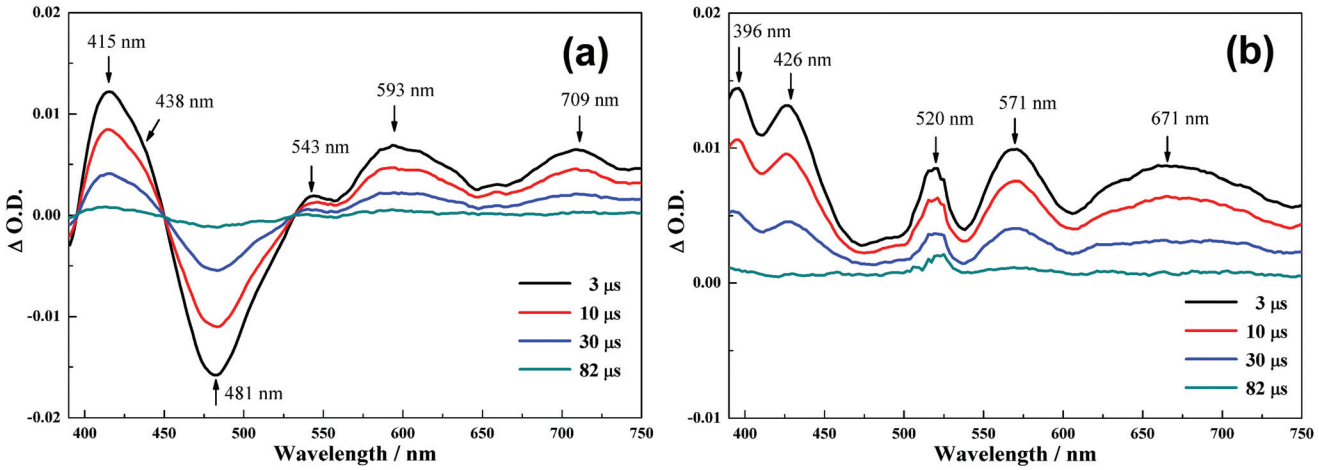

Fig. 2 Nanosecond time-resolved transient difference absorption spectra of (a) C_{70} and (b) bodipy–C_{70} (photoexcitation at 532 nm, 6.9 mJ per pulse power, c[photosensitizer] = 1.0×10^{-5} M in deaerated toluene, 25 °C).

ISC of the C_{70} unit, and the triplet state (T_1) is exclusively localized on the C_{70} unit. By fitting the decay of the peak intensity at 671 nm with a double-exponential function, the natural lifetime τ_0 of bodipy–$^3C_{70}$* was determined as *ca.* 80 μs.

Interestingly, both ground-state bleaching bands of bodipy and C_{70} units disappeared as shown in Fig. 2(b). Since all curves in Fig. 2(b) were recorded after a 3 μs delay time, it was reasonably difficult to observe the ground-state bleaching for the bodipy unit because the singlet–singlet energy transfer from bodipy to C_{70} moieties was very fast (usually in a timescale of picoseconds). Moreover, the disappeared ground-state bleaching band of the C_{70} unit might be covered by the nearby triplet–triplet absorption. As shown in Table S2 and Fig. S13,† the ground state absorption of the C_{70} unit became much weaker after derivatization. In addition, the triplet–triplet transition of the C_{70} moiety at 543 nm was blue-shifted to 520 nm for the dyad, and concealed the ground-state bleaching peak.

In the presence of perylene, the bimolecular TTET occurred between perylene and the triplet dyad. The corresponding quantum efficiency, Φ_{TTET}, could be determined by using eqn (1), without taking into account the weak phosphorescence emission.

$$\Phi_{TTET} = \frac{k_{TTET} \cdot [\text{perylene}]}{k_{TTET} \cdot [\text{perylene}] + k_{NR}} = \frac{1/\tau - 1/\tau_0}{1/\tau} \quad (1)$$

where k_{NR} is the rate constant for the non-radiative processes including collision and internal conversion, and k_{TTET} is the quenching rate constant of the triplet photosensitizer by perylene. k_{NR} could be determined as $k_{NR} = 1/\tau_0$. k_{TTET}·[perylene] was expressed by $(1/\tau - 1/\tau_0)$, where τ_0 and τ are the lifetimes of the triplet dyad in the absence and presence of perylene, respectively. The apparent lifetime of bodipy–$^3C_{70}$*, τ, was obtained by fitting the decay rate of absorption at 671 nm at different perylene concentrations (Fig. S3 and Table S1†). Fig. 3(a) shows the linear Stern–Volmer relationship between

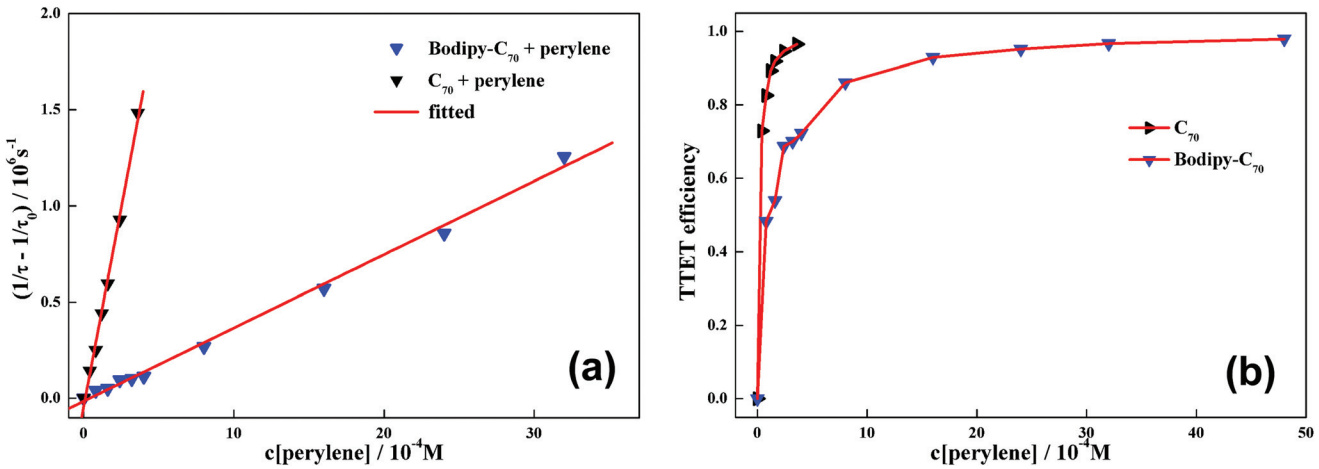

Fig. 3 (a) Stern–Volmer plots describing the effect of the perylene concentration on the lifetime quenching of triplet photosensitizers (bodipy–C_{70} or C_{70}). (b) Triplet–triplet energy transfer (TTET) efficiency as a function of the perylene concentration (excitation at 532 nm, 6.9 mJ per pulse power, c[photosensitizer] = 1.0×10^{-5} M in deaerated toluene, 25 °C).

Table 1 Photophysical parameters of C_{70}, bodipy–C_{70} and bodipy–C_{60} dyad

Compound	λ_{abs} [a]	ε [b]	τ_0 [c]	k_q [d]	Φ_{UC} [e]	η [f]
C_{70}	471	2.1	74.1 ± 5.2	4.13 ± 0.12	24.8 ± 1.0	2404
Bodipy–C_{70}	518	8.2	79.6 ± 6.1	0.38 ± 0.01	10.3 ± 0.5	4417
Bodipy–C_{60} [g]	518–557	4.1–8.1	33.7–39.8	0.51–0.58	4.99–7.95	1497–4690

[a] Absorption peak position, nm. [b] Maximal molar absorption coefficient with the unit of 10^{-4} M^{-1} cm^{-1}. [c] Natural lifetime of the triplet photosensitizer, μs. [d] Bimolecular quenching rate with the unit of 10^9 M^{-1} s^{-1}. [e] Upconversion quantum yield, with a power density of 5000 mW cm^{-2} and c[perylene] = 3.2×10^{-3} M. [f] Overall upconversion capability ($\eta = \varepsilon'\Phi_{UC}$, M^{-1} cm^{-1}) in toluene, c[photosensitizer] = 1×10^{-5} M, ε' was the molar absorption coefficient at 532 nm. [g] The values were cited from ref. 35 and varied depending on the extension of the π-conjugated structure of the bodipy derivative.

$1/\tau - 1/\tau_0$ and the perylene concentration. Based on the plots, the bimolecular quenching rate constant, k_q, was determined as 3.8×10^8 M^{-1} s^{-1} (Table 1). Compared with similar dyads, bodipy–C_{60} ($k_q \sim 5.8 \times 10^8$ M^{-1} s^{-1}),[35] the rate constant of bodipy–C_{70} was slightly smaller. It is natural that the photosensitizer with the smaller size is usually more efficient in the TTET process, because its diffusion is easier. Similar results have been observed by Zhao *et al.*[33] where the C_{60} monomer showed a more efficient TTET quantum yield than its derivatives.

Interestingly, the k_q of the C_{70} monomer as a triplet photosensitizer was much larger than that of bodipy–C_{70}, reflecting the fact that the bodipy unit inevitably hindered the collision of perylene and the C_{70} unit, and reduced the TTET rate. As shown in Fig. 3(b), the TTET efficiencies, Φ_{TTET}, of both C_{70} and bodipy–C_{70} gradually approached 100% with the increasing perylene concentration. In the following TTA experiments, the concentration of perylene was kept constant at 3.2×10^{-3} M to saturate the TTET efficiency, making TTA the rate-determining step of the overall process.

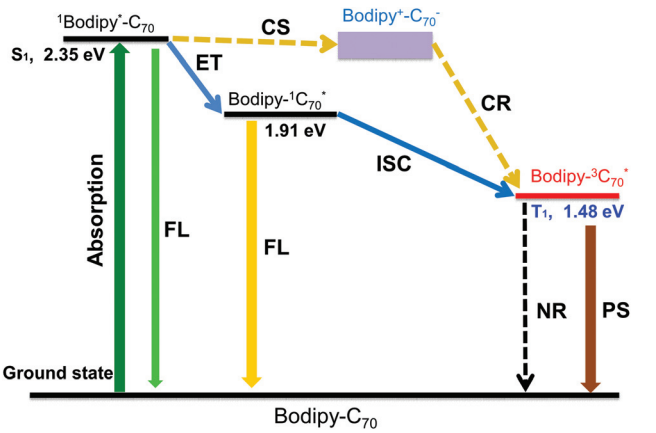

Scheme 3 Jablonski diagram of the bodipy–C_{70} dyad, where ET is singlet-to-singlet energy transfer, ISC is intersystem crossing, CS is charge-separation, CR is charge-recombination, NR is non-radiation, FL is fluorescence emission and PS is phosphorescence. The noted energies were those in toluene, and the excitation energy of bodipy$^+$–C_{70}^- varied with solvents.

Cyclic voltammogram and Gibbs free energy changes

We know that the transformation from ^{1}bodipy*–C_{70} to bodipy–$^3C_{70}$* normally occurs in two steps: the singlet–singlet energy transfer from ^{1}bodipy*–C_{70} to bodipy–$^1C_{70}$* followed by the ISC of the C_{70} unit. However, according to the low reduction potential of C_{70}, the electron transfer between the bodipy and C_{70} units might occur. Then, the produced charge-separated state (CSS) of bodipy$^+$–C_{70}^- could transform to the triplet bodipy–$^3C_{70}$* *via* a charge recombination (CR) as shown in Scheme 3. Obviously, the CSS-mediated transformation was entirely different from the energy transfer mechanism. To evaluate the possibility of intramolecular electron transfer, cyclic voltammograms (CVs) were recorded to obtain the redox potentials of bodipy-B, C_{70} and the bodipy–C_{70} dyad.

Fig. 4 shows the recorded CV curves in Ar-saturated DCM solution containing 0.1 M Bu_4NPF_6 as a supporting electrolyte at 20 °C. The working electrode was the glassy carbon electrode, the counter electrode was the Pt electrode, and the reference electrode was the $Ag/AgNO_3$ electrode. The scan rates were 0.05 V s^{-1}.

In Fig. 4, bodipy-B showed a reversible oxidation wave at +1.12 V and a reversible reduction wave at −1.32 V. There was no oxidation band observed for the C_{70} monomer, but three reversible reduction waves clearly existed at −0.60 V, −0.99 V and −1.41 V, respectively, which were consistent with the previous results.[42] For the bodipy–C_{70} dyad, the reversible oxidation wave at +1.18 V was similar to that of bodipy-B itself. Four reversible reduction waves were located at −0.77 V, −1.15 V, −1.30 V and −1.58 V, respectively. Among them, the one-electron reductions of the bodipy–C_{70} dyad at −0.77 V and −1.15 V could be naturally ascribed to the reduction of the C_{70} moiety, which was anodically shifted by 170 mV and 160 mV from those of the C_{70} monomer. The one-electron reduction at −1.30 V could be attributed to the reduction of the bodipy unit by an anodical shift of 20 mV. These experimental results suggested that the bodipy and C_{70} units acted like the electron donor and acceptor, respectively. As summarized in Table 2, the CV experimental data show that the C_{70} unit in the dyad did not significantly affect the redox potential of the bodipy unit, indicating that the electronic interactions between bodipy and C_{70} units in the ground state were weak.[43] It was consistent with the deduction of the absorption spectra.

Using the redox potentials and the optimized molecular geometries, the thermodynamic driving forces for the charge-

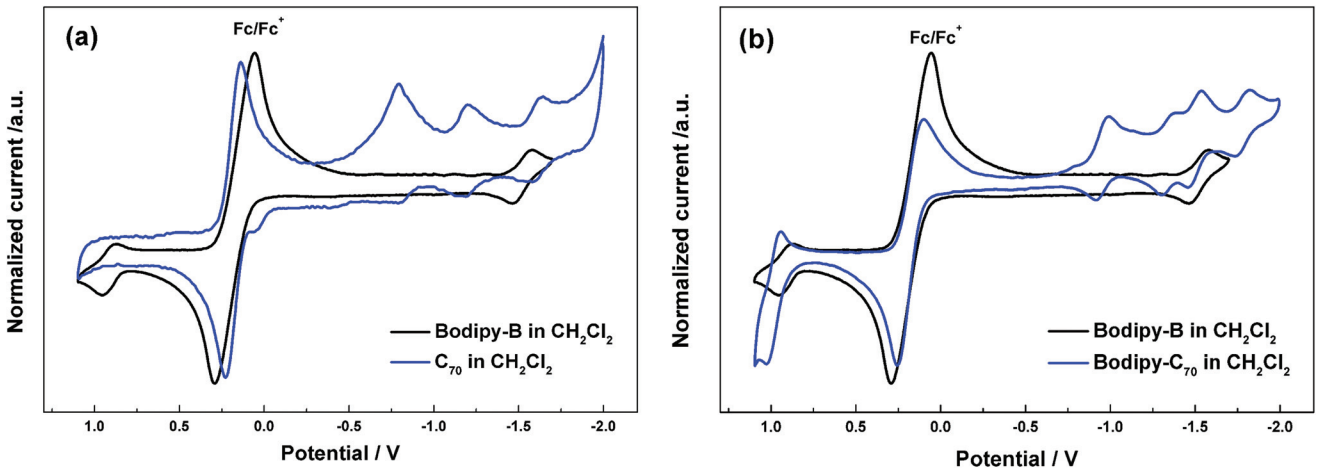

Fig. 4 Cyclic voltammograms of bodipy-B, C_{70} and bodipy–C_{70} in deaerated DCM solution at 20 °C, where ferrocene (Fc) and Ag/$AgNO_3$ reference electrodes were used, with 0.1 M Bu_4NPF_6 as a supporting electrolyte. The scan rate was 0.05 V s^{-1}.

Table 2 Electrochemical redox potentials of C_{70}, bodipy-B and the bodipy–C_{70} dyad[a]

Compound	*E*(ox)/V	*E*(red)/V
Bodipy-B	+1.12	−1.32
C_{70}	—	−0.60, −0.99, −1.41
Bodipy–C_{70}	+1.18	−0.77, −1.15, −1.30, −1.58

[a] Cyclic voltammetry in Ar saturated DCM containing a 0.1 M Bu_4NPF_6 as a supporting electrolyte. The working electrode was the glassy carbon electrode, the counter electrode was the Pt electrode, and the reference electrode was the Ag/$AgNO_3$ electrode. Scan rates: 0.05 V s^{-1}, 20 °C. Ferrocene (Fc) was used as an internal reference ($E_{1/2}$ = +0.38 V) *vs.* saturated calomel electrode (SCE).

recombination (ΔG_{CR}), charge-separation (ΔG_{CS}) and charge-separated state energy (E_{CSS}) of the bodipy–C_{70} dyad were calculated by using the following Weller eqn (2)–(4).

$$\Delta G_{CR} = -[E_{OX}(BDP^+/BDP) - E_{RED}(C_{70}/C_{70}^-)] - \Delta G_s \quad (2)$$

$$\Delta G_{CS} = -\Delta G_{CR} - \Delta E_{0\text{-}0} \quad (3)$$

$$E_{CSS} = [E_{OX}(BDP^+/BDP) - E_{RED}(C_{70}/C_{70}^-)] + \Delta G_s \quad (4)$$

where $E_{OX}(BDP^+/BDP)$ is the half-wave potential for one-electron oxidation of the electron donor bodipy unit, $E_{RED}(C_{70}^-/C_{70})$ is the half-wave potential for the one-electron reduction of the electron acceptor C_{70} unit, $\Delta E_{0\text{-}0}$ is the crossing point of the absorption and fluorescence spectra (*e.g.* 2.37 eV for bodipy–C_{70}) and ΔG_s is the static coulombic energy, which could be calculated using the dielectric continuum model as eqn (5).

$$\Delta G_s = -\frac{e^2}{4\pi\varepsilon_0\varepsilon_s R_{CC}} - \frac{e^2}{8\pi\varepsilon_0}\left(\frac{1}{R_D} + \frac{1}{R_A}\right)\left(\frac{1}{\varepsilon_{REF}} - \frac{1}{\varepsilon_s}\right) \quad (5)$$

where e is the electronic charge, and ε_0, ε_S and ε_{REF} represent the vacuum permittivity, and the dielectric constants of the solvent and the reference, respectively. In the present experiments, the solvents were dichloromethane (ε_S = 9.1) and toluene (ε_{REF} = 2.24). R_{CC} was the center-to-center distance between the electron donor and the electron acceptor, which was 13.7 Å in the bodipy–C_{70} dyad suggested by the DFT optimized geometry (described in section of DFT calculations). R_D and R_A represent the radii of the electron donor and the electron acceptor, and they were estimated to be 6.1 Å and 7.7 Å in the dyad by using the maximum extension radius of the molecular electron cloud in space.

In toluene, the ΔG_S, ΔG_{CS} and ΔG_{CR} were calculated to be +0.50, +0.08, and −2.45 eV, respectively. The energy of the charge-separated state, E_{CSS}, was +2.45 eV, even higher than that of ^{1}bodipy*–C_{70}. The positive Gibbs free energy for charge-separation indicated that the photo-induced electron transfer was thermodynamically prohibited. Therefore, the fluorescence quenching of the bodipy unit in the dyad stemmed from the energy transfer rather than the electron transfer.

DFT calculations on the absorption spectra of bodipy–C_{70}

The photophysical properties of bodipy–C_{70} were calculated using the time-dependent density functional theory. The optimized ground state geometry and the molecular electrostatic potential map of bodipy–C_{70} are shown in Fig. 5(a) and (b). The macrocyclic bodipy was flat and the aromatic rings around bodipy were slightly tilted. The electron cloud was mainly distributed around the boron atom of the bodipy unit, and thus the center-to-center distance between the electron donor and the electron acceptor was the distance between the boron atom and the center of C_{70}, 13.7 Å. Moreover, the frontier molecular orbitals in the singlet and triplet excited states of bodipy–C_{70} were analyzed at the same level as the optimized geometry, and are shown in Fig. 5(c). The HOMO of the dyad was contributed to by the bodipy unit, while the LUMO and LUMO+1 belonged to the C_{70} moiety. The lowest unoccupied molecular orbital of the bodipy unit was designated as LUMO+3 due to

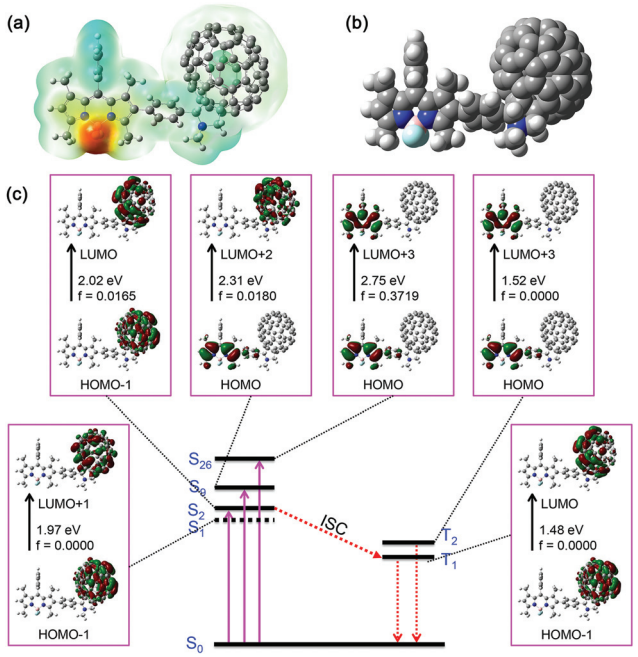

Fig. 5 (a) Space filling model and (b) molecular electrostatic potential map of the bodipy–C_{70} dyad geometry optimized with the B3LYP/6-31G (d) level. (c) The frontier orbitals involved in the singlet and triplet excited states of bodipy–C_{70}. Toluene was used as a solvent in the calculations.

its higher energy. Thus, the photo-absorption of the bodipy moiety in the dyad at 532 nm was expected to be contributed to by the transition from the HOMO to LUMO+3. Additionally, the transition had a significant oscillator strength compared with the nearby transitions as shown in Fig. 5(c).

Table 3 summarizes the calculated transition energies, oscillator strengths and main electronic configurations of the low-lying singlet and triplet states of the dyad. Based on these calculated data, the UV-Vis absorption spectra could be assigned. Although the calculated transition energy of the strongest absorption band ($S_0 \rightarrow S_{26}$, S_{27}) was larger than the experimental data (2.394 eV, 518 nm), the configuration property of the first band was assigned to the transition of HOMO → LUMO+3 as we expected. Moreover, the energy gap between the ground state S_0 and the lowest triplet state T_1 was 1.48 eV and close to the energy of triplet C_{70}. As shown in Table 1, the major electronic configuration of T_1 corresponded to the transition of HOMO−1 → LUMO. Therefore, the lowest triplet state, T_1, was localized on the C_{70} unit. Both the spin density calculation and the nanosecond time-resolved transient absorption spectra also confirmed the conclusion.

Triplet–triplet annihilation upconversion of perylene

In the presence of perylene, the upconverted fluorescence was observed due to the TTA-UC process, when bodipy–C_{70} or C_{70} itself was used as the triplet photosensitizer. Both the upconverted fluorescence intensities were gradually enhanced with the increase of the excitation power density, as shown in Fig. 6(a). The double logarithmic plot for the bodipy–C_{70} photosensitizer shown in Fig. 6(b) indicates that the slope at a lower power density was close to 2, and gradually decreased to unity at higher power densities.[44] The threshold power density I_{th} for the bodipy–C_{70} dyad was determined as 163 mW cm^{-2} as the turning point shown in Fig. 6(b).

Using the fluorescence of I_2-bodipy[24,32] as the standard (Φ_{std} = 2.7% in ACN), the TTA-UC quantum yields, Φ_{UC}, were determined by using eqn (6),

$$\Phi_{UC} = 2 \cdot \Phi_{std} \cdot \left(\frac{A_{std}}{I_{std}}\right) \cdot \left(\frac{I_{sam}}{A_{sam}}\right) \cdot \left(\frac{\eta_{sam}}{\eta_{std}}\right)^2 \quad (6)$$

where A, I and n are the absorbance intensity, the integrated luminescence intensity, and the refractive index of the solvents used for the standard and the samples. In the equation, a factor of 2 was multiplied in order to make the maximum quantum yield 100%. The Φ_{UC} values for both photosensitizers

Table 3 Transition energies, wavelengths (λ), oscillator strengths (f), major electronic configurations and CI coefficients of the low-lying electronic excited states of bodipy–C_{70}, calculated at the TD-DFT//B3LYP/6-31G(d) level[a]

State	Transition	Energy/λ	f[b]	Configuration[c]	CI
Singlet	$S_0 \rightarrow S_1$	1.97 eV/628.8 nm	0.0000	HOMO−1 → LUMO+1	0.69582
	$S_0 \rightarrow S_2$	2.02 eV/613.5 nm	0.0165	HOMO−1 → LUMO	0.65926
	$S_0 \rightarrow S_9$	2.31 eV/535.7 nm	0.0180	HOMO → LUMO+2	0.54381
	$S_0 \rightarrow S_{10}$	2.33 eV/531.7 nm	0.0661	HOMO−2 → LUMO+1	0.37553
				HOMO−3 → LUMO+2	0.28605
	$S_0 \rightarrow S_{26}$	2.75 eV/451.1 nm	0.3719	HOMO → LUMO+3	0.48239
				HOMO → LUMO+4	0.46382
	$S_0 \rightarrow S_{27}$	2.75 eV/450.1 nm	0.3411	HOMO → LUMO+3	0.44850
				HOMO → LUMO+4	0.48745
Triplet	$S_0 \rightarrow T_1$	1.48 eV/839.9 nm	0.0000	HOMO−1 → LUMO	0.48474
				HOMO−1 → LUMO+1	0.32694
	$S_0 \rightarrow T_2$	1.52 eV/816.8 nm	0.0000	HOMO → LUMO+3	0.69640
	$S_0 \rightarrow T_3$	1.67 eV/743.0 nm	0.0000	HOMO−1 → LUMO	0.38788
				HOMO−1 → LUMO+1	0.30945

[a] Only the low-lying excited states with the larger oscillator strength are listed. [b] No spin–orbital coupling was considered, and thus the f values for the triplet bands are zero. [c] The major configurations are shown.

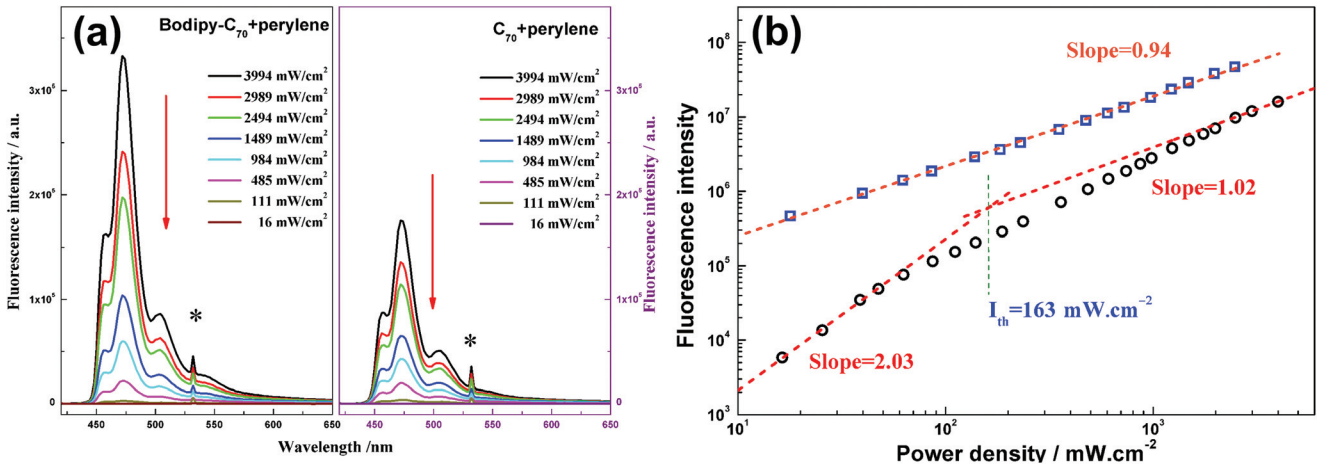

Fig. 6 (a) Upconverted fluorescence emission spectra of perylene with the photosensitizer of bodipy–C_{70} and C_{70} at various excitation power densities. (b) Double logarithmic plot of the upconverted fluorescence intensity as a function of the excitation power density for bodipy–C_{70}, as well as the linear dependence of the normal fluorescence of bodipy-B. *c*[photosensitizer] = 1 × 10^{-5} M, *c*[perylene] = 3.2 × 10^{-3} M, in deaerated toluene at 25 °C.

were determined as 24.8% for C_{70}/perylene and 10.3% for bodipy–C_{70}/perylene. Although bodipy–C_{70} has a slower bimolecular quenching rate than bodipy–C_{60} according to its bigger size (in Table 1), the Φ_{UC} of bodipy–C_{70} is much higher than that of bodipy–C_{60}. It is emphasized that the TTA upconversion is a multi-step process, and all the characteristics involving the TTET rate and the lifetime of the triplet sensitizer should be taken into account equally. Moreover, Zhao *et al.*[45] suggested that the light-harvesting ability of the photosensitizer should also be taken into account, proposing the overall upconversion capability, $\eta = \varepsilon \cdot \Phi_{UC}$ (ε is the molar extinction coefficient), as a better evaluation parameter. Thus, the η values for C_{70}/perylene and bodipy–C_{70}/perylene systems were 2404 M^{-1} cm^{-1} and 4417 M^{-1} cm^{-1}, respectively. Interestingly, although the Φ_{UC} of bodipy–C_{70} was only about half of that of C_{70}, the overall capability of the former exceeded that of the latter by nearly a factor of two, *i.e.*, bodipy–C_{70} was a better triplet photosensitizer than the parent C_{70}.

For the practical applications, the optical stability of photosensitizers with a long-term exposure was very important but rarely investigated. As shown in Fig. 7(a), the upconverted fluorescence intensity of C_{70}/perylene quickly decreased with time, while that of bodipy–C_{70}/perylene was kept constant during the first 20 min, and then slowly decreased to 79% after 60 min exposure at 532 nm with a power density of 4000 mW cm^{-2}. Thus, bodipy–C_{70} was more stable as a triplet

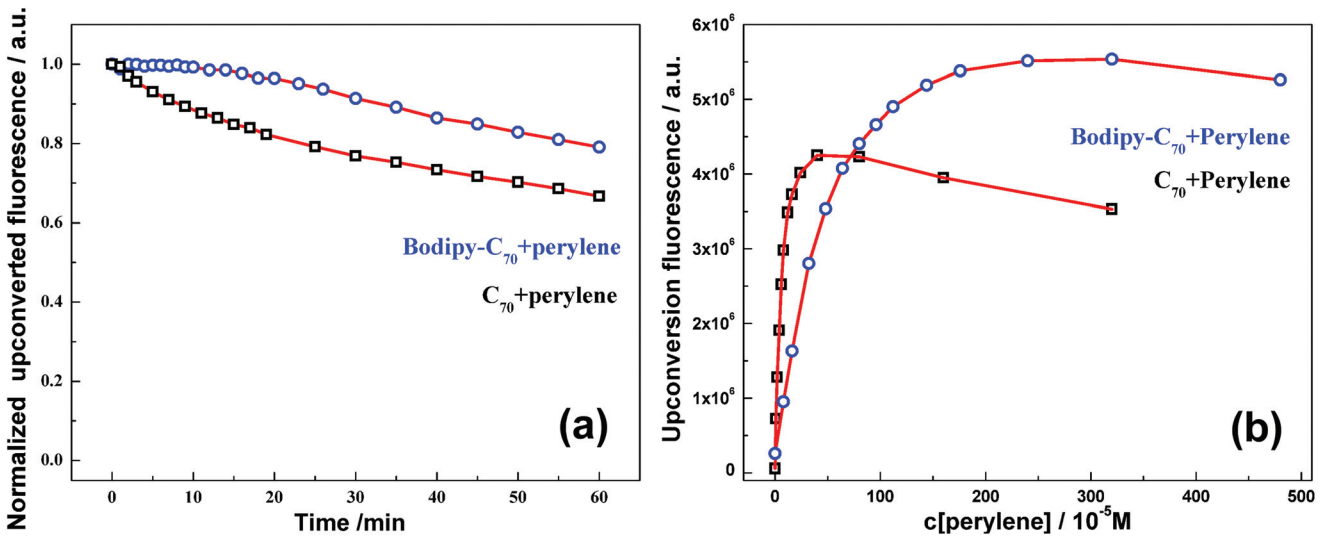

Fig. 7 (a) Normalized upconverted fluorescence intensities of bodipy–C_{70} and C_{70} as functions of laser exposure time (532 nm, 4000 mW cm^{-2}), *c*[photosensitizer] = 1 × 10^{-5} M, and *c*[perylene] = 3.2 × 10^{-3} M. (b) Dependence of the upconverted fluorescence intensity on perylene concentration, *c*[photosensitizer] = 1 × 10^{-5} M, 532 nm, 2000 mW cm^{-2}, in deaerated toluene at 25 °C.

photosensitizer than C_{70} under long-time intense laser irradiation.

As the TTA process occurred between two triplet perylene molecules, the high concentration of perylene was beneficial in improving the TTA quantum yield. However, the self-quenching of the energy acceptor at high concentrations probably weakened the improvement. Moreover, the generation of a triplet excimer had been verified recently in a fullerene/functionalized Pt(II) metallacycle (C_{60}/Pt) TTA upconversion system, with the triplet excited state emission observed at high concentrations.[46] Thus, the concentration effect should also be considered in the present system. As shown in Fig. 7(b), the upconverted fluorescence intensities of bodipy–C_{70} and/or C_{70} were measured at different perylene concentrations, and the results clearly showed the dependence. At low concentrations, the upconverted fluorescence intensities rapidly increased to the maximum with the increasing concentration, and then slightly decreased at a high concentration. However, no phosphorescence emission was observed in the experiment, indicating that the triplet excimer production did not dominate at a high concentration.

Conclusion

As a new metal-free organic photosensitizer for TTA upconversion of perylene, the bodipy–C_{70} dyad was synthesized and applied. The bodipy–C_{70} dyad showed a strong absorption in the visible region with the maximal molar extinction coefficient of up to 82 300 mol^{-1} cm^{-1} at 518 nm. The absorption and fluorescence spectra suggested that the singlet–singlet energy transfer between bodipy and C_{70} units was very efficient with a quantum yield of nearly 100%. Subsequently, the lowest triplet state of the dyad was populated *via* the ISC of the C_{70} moiety, with a long lifetime of *ca.* 80 μs in toluene. The nanosecond transient absorption spectra and theoretical calculations demonstrated that the lowest triplet state of the dyad was located in the C_{70} unit. In the electrochemical investigation, a positive ΔG_{CS} for charge-separation was obtained, indicating that the intramolecular electron transfer of the dyad was thermodynamically prohibited in toluene.

Compared to bromo- or iodo-bodipy (ISC efficiency is less than 83%),[25,27] the ISC efficiency of bodipy–C_{70} is up to ~100%. Moreover, the lifetime of triplet bodipy–C_{70} is *ca.* 80 microseconds, which is much longer than that of bodipy–C_{60} (~30 microseconds[35]). Thus, the bodipy–C_{70} dyad looks like an excellent triplet photosensitizer. In the presence of perylene as the triplet energy acceptor and emitter, the TTA upconverted fluorescence was clearly observed with a maximum quantum yield of 10.3% in toluene. The overall upconversion capability of 4417 M^{-1} cm^{-1} exceeded that of C_{70} approximately two-fold. Moreover, the bodipy–C_{70} dyad also exhibited an enhanced optical stability under intense irradiation. All data indicated that the dyad was a more ideal photosensitizer for the TTA upconversion of perylene in the fullerene derivative family.

Experimental section

Synthesis and characterization of the bodipy–C_{70} dyad

C_{70} (99%) and perylene (98%) were purchased from Aladdin Industrial Co. Toluene (AR, >99.5%) and chlorobenzene (AR, >99.5%) were bought from Sinopharm Chemical Reagent Co. Ltd and used without any purification.

Bodipy and bodipy-CHO were prepared as described in the references.[35,47] Then, the bodipy–C_{70} dyad was synthesized *via* the Prato reaction of bodipy-CHO and sarcosine with C_{70}. Under an argon atmosphere, bodipy-CHO (25.5 mg, 0.06×10^{-3} mol), sarcosine (53 mg, 0.6×10^{-3} mol) and C_{70} (50 mg, 0.06×10^{-3} mol) were suspended in dry chlorobenzene (50 mL). The solution was heated and refluxed for 12 h with stirring. After cooling to room temperature, the solvent was evaporated under reduced pressure. The residue was purified by column chromatography (silica gel, cyclohexane → cyclohexane/toluene(1 : 1) → toluene) to give the product bodipy–C_{70} as a brick red solid (7.9 mg, 11%). ^{1}H NMR (400 MHz, $CDCl_3$): δ 7.49–7.43 (m, 3H), 7.42–7.26 (m, 4H), 7.04 (t, J = 20.2 Hz, 2H), 5.98 (s, 1H), 4.31 (s, 1H), 4.18 (s, 1H), 3.59 (d, J = 9.1 Hz, 1H), 2.55 (s, 3H), 2.48 (s, 3H), 2.36 (s, 3H), 1.35 (s, 3H), 1.13 (s, 3H). MALDI-MS: calcd ($[C_{98}H_{28}BF_2N_3]^+$) m/z = 1296.24, found m/z = 1296.26.

Steady-state and transient absorption and fluorescence emission spectra

The steady-state UV-Vis absorption spectra were recorded in a wavelength range of 300–700 nm using a spectrophotometer (UV-3600, Shimadzu). The fluorescence emission was measured using a fluorescence spectrophotometer (F-4600, Hitachi) in a wavelength range of 400–800 nm.

Nanosecond time-resolved transient absorption spectra were recorded using a home-built laser flash photolysis system. The second harmonic (532 nm) of a Q-Switched Nd:YAG laser (PRO-190, Spectra Physics) was utilized as the excitation source (pulse duration: 8 ns, repetition rate: 10 Hz, pulse energy < 10 mJ per pulse). A 500 W xenon lamp was used as the source of the analyzing light, and passed through a flow quartz cuvette perpendicularly to the pulsed laser. The optical absorption path length was 10 mm. A monochromator equipped with a photomultiplier (CR131, Hamamatsu) was employed to record the transient absorption spectra within a wavelength range of 320–700 nm. The typical spectral resolution was less than 1 nm. A dynamic decay curve of the intermediate was averaged by multi-shots and recorded using an oscilloscope (TDS3052B, Tektronix). All the solutions were deoxygenated by purging with high purity argon (99.99%) for about 20 minutes prior to measurements.

TTA upconversion spectra

A stable CW laser (Verdi-V5, 532 nm, Coherent) was used as the excitation light source. The diameter of the laser spot is *ca.* 5 mm. In the TTA UC experiment, the solution was deoxygenated by purging with high-purity helium for at least 20 minutes, and the gas flow was maintained during the

measurement. With photoexcitation at 532 nm, the upconverted fluorescence of perylene was dispersed and detected using a commercial monochromator system (Triplepro, Acton Research) and a CR131 photomultiplier. The spectral resolution was *ca.* 1.0 nm.

Cyclic voltammetry

Cyclic voltammograms were recorded with a scan rate of 50 mV s^{-1}. A three-electrode electrolytic cell was used, with 0.1 M tetrabutylammonium hexafluorophosphate ($Bu_4N[PF_6]$) as a supporting electrolyte. The working electrode was a glassy carbon electrode, and the counter electrode was a platinum electrode. A non-aqueous $Ag/AgNO_3$ (0.1 M in acetonitrile) reference electrode was contained in a separate compartment connected to the solution *via* a semipermeable membrane. DCM was used as the solvent. Ferrocene was added as the internal reference. Electrochemical measurements were carried out at room temperature after purging with argon for 30 minutes.

Quantum chemical calculations

Molecular geometries were optimized using density functional theory at the B3LYP/6-31G(d) level. No imaginary frequencies were found for the optimized structures. The spin density surfaces of the dyad were calculated at the same level of theory, and the energy gaps between its ground state and the excited states were calculated. The vertical excitation energies were compared with the experimental data in the absorption spectra, and the corresponding transitions of spectral bands were assigned. The PCM model was utilized to evaluate the solvent effect. All these calculations were performed using the Gaussian 09 W program package.[48]

Conflicts of interest

There are no conflicts to declare.

Acknowledgements

This work was supported by the National Natural Science Foundation of China (Grant No. 21573210 and 21573208) and the National Key Basic Research Foundation (Grant No. 2013CB834602). The quantum chemical calculations in this study were performed on the supercomputing system in the Supercomputing Center of the University of Science and Technology of China. X. Zhou also thanks the National Key Research and Development program (Grant No. 2016YFF0200502) for support.

References

1 A. Nattestad, Y. Y. Cheng, R. W. MacQueen, T. F. Schulze, F. W. Thompson, A. J. Mozer, B. Fuckel, T. Khoury, M. J. Crossley, K. Lips, G. G. Wallace and T. W. Schmidt, *J. Phys. Chem. Lett.*, 2013, **4**, 2073–2078.
2 Y. Y. Cheng, B. Fückel, R. W. MacQueen, T. Khoury, R. G. Clady, T. F. Schulze, N. J. Ekins-Daukes, M. J. Crossley, B. Stannowski, K. Lips and T. W. Schmidt, *Energy Environ. Sci.*, 2012, **5**, 6953–6953.
3 C. Li, C. Koenigsmann, F. Deng, A. Hagstrom, C. A. Schmuttenmaer and J.-H. Kim, *ACS Photonics*, 2016, **3**, 784–790.
4 C. Ye, J. Wang, X. Wang, P. Ding, Z. Liang and X. Tao, *Phys. Chem. Chem. Phys.*, 2016, **18**, 3430–3437.
5 B. Wang, B. Sun, X. Wang, C. Ye, P. Ding, Z. Liang, Z. Chen, X. Tao and L. Wu, *J. Phys. Chem. C*, 2014, **118**, 1417–1425.
6 H.-i. Kim, S. Weon, H. Kang, A. L. Hagstrom, O. S. Kwon, Y.-S. Lee, W. Choi and J.-H. Kim, *Environ. Sci. Technol.*, 2016, **50**, 11184–11192.
7 M. Haring, R. Perez-Ruiz, A. Jacobi von Wangelin and D. D. Diaz, *Chem. Commun.*, 2015, **51**, 16848–16851.
8 Q. Liu, T. Yang, W. Feng and F. Li, *J. Am. Chem. Soc.*, 2012, **134**, 5390–5397.
9 Y. Liu, Q. Su, X. Zou, M. Chen, W. Feng, Y. Shi and F. Li, *Chem. Commun.*, 2016, **52**, 7466–7469.
10 Q. Liu, B. Yin, T. Yang, Y. Yang, Z. Shen, P. Yao and F. Li, *J. Am. Chem. Soc.*, 2013, **135**, 5029–5037.
11 P. Zhang, C. Shao, Z. Zhang, M. Zhang, J. Mu, Z. Guo and Y. Liu, *Nanoscale*, 2011, **3**, 3357–3363.
12 M. Haase and H. Schäfer, *Angew. Chem., Int. Ed.*, 2011, **50**, 5808–5829.
13 A. Monguzzi, R. Tubino, S. Hoseinkhani, M. Campione and F. Meinardi, *Phys. Chem. Chem. Phys.*, 2012, **14**, 4322–4332.
14 S. Baluschev, T. Miteva, V. Yakutkin, G. Nelles, A. Yasuda and G. Wegner, *Phys. Rev. Lett.*, 2006, **97**, 143903.
15 F. Deng, J. Blumhoff and F. N. Castellano, *J. Phys. Chem. A*, 2013, **117**, 4412–4419.
16 Y. Y. Cheng, B. Fuckel, T. Khoury, R. G. Clady, N. J. Ekins-Daukes, M. J. Crossley and T. W. Schmidt, *J. Phys. Chem. A*, 2011, **115**, 1047–1053.
17 W. Wu, L. Liu, X. Cui, C. Zhang and J. Zhao, *Dalton Trans.*, 2013, **42**, 14374–14379.
18 S. Baluschev, V. Yakutkin, T. Miteva, Y. Avlasevich, S. Chernov, S. Aleshchenkov, G. Nelles, A. Cheprakov, A. Yasuda, K. Mullen and G. Wegner, *Angew. Chem., Int. Ed.*, 2007, **46**, 7693–7696.
19 Y. Sasaki, S. Amemori, H. Kouno, N. Yanai and N. Kimizuka, *J. Mater. Chem. C*, 2017, **5**, 5063–5067.
20 J. Wang, Y. Lu, N. McGoldrick, C. Zhang, W. Yang, J. Zhao and S. M. Draper, *J. Mater. Chem. C*, 2016, **4**, 6131–6139.
21 P. Majumdar, X. Yuan, S. Li, B. Le Guennic, J. Ma, C. Zhang, D. Jacquemin and J. Zhao, *J. Mater. Chem. B*, 2014, **2**, 2838–2854.
22 Y. You, *Org. Biomol. Chem.*, 2016, **14**, 7131–7135.
23 C. Zhang and J. Zhao, *J. Mater. Chem. C*, 2016, **4**, 1623–1632.

24 Q. Zhou, M. Zhou, Y. Wei, X. Zhou, S. Liu, S. Zhang and B. Zhang, *Phys. Chem. Chem. Phys.*, 2017, **19**, 1516–1525.
25 Z. Mahmood, K. Xu, B. Kucukoz, X. Cui, J. Zhao, Z. Wang, A. Karatay, H. G. Yaglioglu, M. Hayvali and A. Elmali, *J. Org. Chem.*, 2015, **80**, 3036–3049.
26 J. Zhao, K. Chen, Y. Hou, Y. Che, L. Liu and D. Jia, *Org. Biomol. Chem.*, 2018, **16**, 3692–3701.
27 L. Jiao, W. Pang, J. Zhou, Y. Wei, X. Mu, G. Bai and E. Hao, *J. Org. Chem.*, 2011, **76**, 9988–9996.
28 A. N. Amin, M. E. El-Khouly, N. K. Subbaiyan, M. E. Zandler, S. Fukuzumi and F. D'Souza, *Chem. Commun.*, 2012, **48**, 206–208.
29 M. Ince, A. Hausmann, M. V. Martinez-Diaz, D. M. Guldi and T. Torres, *Chem. Commun.*, 2012, **48**, 4058–4060.
30 L. Huang, X. Yu, W. Wu and J. Zhao, *Org. Lett.*, 2012, **14**, 2594–2597.
31 Y. Liu and J. Zhao, *Chem. Commun.*, 2012, **48**, 3751–3753.
32 W. Wu, J. Zhao, J. Sun and S. Guo, *J. Org. Chem.*, 2012, **77**, 5305–5312.
33 P. Yang, W. Wu, J. Zhao, D. Huang and X. Yi, *J. Mater. Chem.*, 2012, **22**, 20273–20283.
34 N. M. Dimitrijevic and P. V. Kamat, *J. Phys. Chem.*, 1992, **96**, 4811–4814.
35 Y. Wei, M. Zhou, Q. Zhou, X. Zhou, S. Liu, S. Zhang and B. Zhang, *Phys. Chem. Chem. Phys.*, 2017, **19**, 22049–22060.
36 C. Fan, W. Wu, J. J. Chruma, J. Zhao and C. Yang, *J. Am. Chem. Soc.*, 2016, **138**, 15405–15412.
37 J. W. Arbogast, A. P. Darmanyan, C. S. Foote, F. N. Diederich, R. Whetten, Y. Rubin, M. M. Alvarez and S. J. Anz, *J. Phys. Chem.*, 1991, **95**, 11–12.
38 J. W. Arbogast and C. S. Foote, *J. Am. Chem. Soc.*, 1991, **113**, 8886–8889.
39 M. Fraelich and R. Weisman, *J. Phys. Chem.*, 1993, **97**, 11145–11147.
40 K. Moor, J.-H. Kim, S. Snow and J.-H. Kim, *Chem. Commun.*, 2013, **49**, 10829–10831.
41 J. P. Hare, H. W. Kroto and R. Taylor, *Chem. Phys. Lett.*, 1991, **177**, 394–398.
42 Q. Xie, E. Perez-Cordero and L. Echegoyen, *J. Am. Chem. Soc.*, 1992, **114**, 3978–3980.
43 R. Ziessel, B. D. Allen, D. B. Rewinska and A. Harriman, *Chem. – Eur. J.*, 2009, **15**, 7382–7393.
44 A. Haefele, J. Blumhoff, R. S. Khnayzer and F. N. Castellano, *J. Phys. Chem. Lett.*, 2012, **3**, 299–303.
45 J. Zhao, S. Ji and H. Guo, *RSC Adv.*, 2011, **1**, 937–950.
46 R. Zhang, Y. Yang, S. Yang, V. S. Neti, H. Sepehrpour, P. J. Stang and K. Han, *J. Phys. Chem. C*, 2017, **121**, 14975–14980.
47 L. Huang, X. Cui, B. Therrien and J. Zhao, *Chem. – Eur. J.*, 2013, **19**, 17472–17482.
48 M. Frisch, G. Trucks, H. B. Schlegel, G. Scuseria, M. Robb, J. Cheeseman, G. Scalmani, V. Barone, B. Mennucci and G. Petersson, *Gaussian 09*, Gaussian. Inc., Wallingford, CT, 2009.

